Nanoscale

Optimizing PtFe Intermetallics for Oxygen Reduction Reaction: From DFT Screening to In-Situ XAFS Characterization

Journal:	*Nanoscale*
Manuscript ID	NR-ART-06-2019-004975.R2
Article Type:	Paper
Date Submitted by the Author:	22-Sep-2019

Complete List of Authors:	Gong, Mingxing; Huazhong University of Science and Technology Zhu, Jing; School of Chemistry and Chemical Engineering, Huazhong University of Science&Technology Liu, Mingjie; Brookhaven National Laboratory Liu, Peifang; Xinyang Normal University Deng, Zhiping; Huazhong University of Science&Technology, School of Chemistry and Chemical Engineering Shen, Tao; Huazhong University of Science and Technology Zhao, Tonghui; School of Chemistry and Chemical Engineering, Huazhong University of Science and Technology Lin, Ruoqian; Brookhaven National Laboratory, Lu, Yun ; Huazhong University of Science and Technology Yang, Shize; Oak Ridge National Laboratory, Materials Science Technology Division; Brookhaven National Laboratory, Liang, Zhixiu; Brookhaven National Laboratory Bak, Seong Min; Brookhaven National Laboratory, Chemistry Division Stavitski, Eli; Brookhaven National Laboratoty, Wu, Qin; Brookhaven National Laboratory, Center for Functional Nanomaterials Adzic, Radoslav; Brookhaven National Laboratory, Xin, Huolin L.; Center for Functional Nanomaterials, Wang, Deli; Huazhong University of Science&Technology, School of Chemistry and Chemical Engineering

Nanoscale

ARTICLE

Optimizing PtFe Intermetallics for Oxygen Reduction Reaction: From DFT Screening to In-Situ XAFS Characterization

Received 00th January 20xx,
Accepted 00th January 20xx

DOI: 10.1039/x0xx00000x

www.rsc.org/

Mingxing Gong,[a] Jing Zhu,[a] Mingjie Liu,[c] Peifang Liu,[b] Zhiping Deng,[a] Tao Shen,[a] Tonghui Zhao,[a] Ruoqian Lin,[c] Yun Lu,[a] Shize Yang,[c] Zhixiu Liang,[d] Seong Min Bak,[d] Eli Stavitski,[e] Qin Wu,[c] Radoslav R. Adzic,[d] Huolin L. Xin,[*, c, f] and Deli Wang[*, a]

Rational designing of catalysts to promote the sluggish kinetics of cathode oxygen reduction reaction in proton exchange membrane fuel cells is still challenging, yet of crucial importance to its commercial application. In this work, on the basis of theoretical DFT calculations which suggest that order structured *fct*-phased PtFe (O-PtFe) with atomic Pt shell exhibits superior electrocatalytic performance towards ORR, the desired structure was prepared by using a scalable impregnation-reduction method. The as-prepared O-PtFe delivered enhanced activity (0.68 A mg^{-1}_{Pt}) and stability (73% activity retention after 10000 potential cycles) compared with the corresponding disorder PtFe alloy (D-PtFe) and Pt. To evidence the excellent durability, in-situ X-ray absorption fine structure spectroscopy was conducted to probe the local and electronic structures change of the O-PtFe during 10,000 cycles accelerated durability testing. We hope this facile synthesis method and the in-situ XAFS experiment could be readily adopted to other catalyst system, facilitating the screening of highly efficient ORR catalyst for fuel cell application.

Introduction

Effectively promoting the sluggish kinetics of cathode oxygen reduction reaction (ORR) in proton exchange membrane fuel cells (PEMFC) is still an open challenge[1-4]. The past decades had witnessed the progress of rational design of ORR catalysts. Among them, Pt-based nanomaterials are still the most promising catalyst for the practical application in the near future due to their relatively high activity and durability when subjected to harsh operating environment[1]. Alloying 3*d* transition metals with Pt was a widely adopted strategy which can not only lower the Pt content but also induce the compressive strain in the lattice of Pt to slightly weaken the bonding strength of oxygenated species[5]. To date, the mass activity (MA) enhancement factor of Pt-based alloys toward ORR varies from 2 to 8 in comparison to that on pure Pt[6, 7]. Additionally, combining with shape and/or surface tune strategies, alloys such as Pt_3Ni nanoframe[8] and transition metal-doped Pt_3Ni octahedral[9] even demonstrated 36-fold and 73-fold enhancement in MA compared with Pt, respectively.

Though superior catalytic activity had been successfully obtained by numerous strategies, the alloying effect also gave rise to undesired problem, viz, poor durability due to the serious dissolution of transition metals (TMs)[10, 11]. As a result, the stability of the Pt-M alloy catalysts is far from to meet the requirement for practical long-term operations. How to stabilize the TMs against leaching from the alloy structure has drawn increasing attention[11-13]. Among all the reported stabilize methods, a promising one is to transform the disordered alloy into an ordered intermetallic structure[14-16]. Generally, when atomically transform into an intermetallic phase, Pt-M intermetallic acquire enhanced stability over conventional alloys with disordered atomic distributions due to the large formation enthalpy and strong Pt(*5d*)-M(*3d*) coupled effect along the *c*-axis[17, 18]. Wang et al reported the long-term stability of the ordered face-centered cubic (*fcc*) Pt_3Co intermetallic nanoparticles and attributed it to the ultrathin Pt rich surface and an ordered intermetallic structure in the core[19]. Chen et. al developed a KCl matrix method[20] and successfully prepared ordered Pt_3M (M=Fe, Ti, Zr, Zn and V) nanoparticles as effective FCs catalysts. Interestingly, ordered PtFe intermetallic nanoparticles with face-centered tetragonal (*fct*) structure in the meantime featured by atomically Pt shell exhibited remarkable activity and Fe anti-leaching property

[a]*Key laboratory of Material Chemistry for Energy Conversion and Storage, Ministry of Education, Hubei Key Laboratory of Material Chemistry and Service Failure, School of Chemistry and Chemical Engineering, Huazhong University of Science and Technology. Wuhan 430074, China. E-mail: wangdl81125@hust.edu.cn*
[b]*Analysis & testing center of Xinyang Normal University, Xinyang 464000, China*
[c]*Center for Functional Nanomaterials, Brookhaven National Laboratory, Upton, 11973, NY, USA.*
[d]*Chemistry Division, Brookhaven National Laboratory, Upton, 11973, NY, USA*
[e]*National Synchrotron Light Source II, Brookhaven National Laboratory, Upton, 11973, NY, USA*
[f]*Department of Physics and Astronomy, University of California, Irvine, 92697, CA, USA*
†Electronic Supplementary Information (ESI) available. See DOI: 10.1039/x0xx00000x

under real operating condition were reported by Sun et al[21, 22]. During the high temperature driven phase transformation of disorder *fcc* to ordered *fct*, transition metal oxide (MgO, NiO, Fe_3O_4) were generally act as barrier to avoid size increasing and sintering of the PtM nanoparticles. Still and all, a slight pity is that the synthesis of ordered PtFe in previously reported work involved a complicated solvothermal process and followed by time consuming MgO coating-removing procedure[23]. A simple and efficient strategy for the preparation of ordered intermetallic PtFe nanoparticles with a Pt skin is highly desired currently.

We present here an impregnation-reduction method for the synthesis of *fcc*-phased PtFe disordered alloy (D-PtFe), the followed annealing processing in hydrogen atmosphere will activate Pt and Fe interdiffusion to *fct*-phased ordered intermetallic structure and induce Pt surface segregation to form an ultrathin strained Pt shell simultaneously (O-PtFe). The as-prepared O-PtFe were well characterizated and the electrocatalytic performance towards ORR were evaluated. Particularly, in-situ X-ray absorption fine structure spectroscopy (in-situ XAFS) was conducted to probe the local and electronic structure of the O-PtFe under 10,000 cycles accelerated durability testing.

Experimental

DFT Calculations.

All DFT calculations were performed using the Vienna *ab* Initio Simulation Package (VASP) with the projector augmented wave (PAW) method and the Perdew, Burke and Ernzerhof (PBE) function. The electron wave function was expanded using plane waves with an energy cutoff of 450 eV. The slab model used for Pt_xFe contains three layers of Pt_xFe and two layers of Pt skin with at least 15 Å vacuum layer. The Pt_xFe (111) surface is constructed with 2×2 supercell for the calculations with adsorbates during ORR process. The Monkhorst-Pack grid is used with 5×5×1 mesh in surface calculations. In geometry relaxation, the bottom layer is fixed and four layers as well as the adsorbates are relaxed until the maximum force is less than 0.01 eV $Å^{-1}$. All calculations are spin polarized.

Reagents.

Chloroplatinic Acid (H_2PtCl_6) and Ferric Chloride ($FeCl_3$) supplied by Sinopharm Chemical Reagent Co., Ltd. (Shanghai, China). Perchloric acid ($HClO_4$) purchased from Aladdin. Other reagents were all of AR grade used without further purification. The water used in this work is ultrapure with a resistivity of 18.2 MΩ.

Catalysts preparation.

The carbon-supported Pt-Fe series nanoparticles with Pt:Fe nominal ratio of 3:1, 1:1 and 1:3 were prepared via an impregnation reduction method. For example, in a typical synthesis of Pt_3Fe, 53.0 mg of $H_2PtCl_6 \cdot 6H_2O$ and 5.5 mg of $FeCl_3$ were simultaneously dissolved in deionized water, and then 78.1 mg of Vulcan XC-72 carbon support were dispersed into the solution. After ultrasonic dispersion for 30 min, the suspension was heated under magnetic stirring to evaporate the solvent and form a smooth, thick slurry. Subsequently, the slurry was dried in a vacuum oven at 60 ℃ for 12 h. After being ground in an agate mortar, the resulting dark powder was heated in a tube furnace at 300 ℃ under flowing H_2/Ar atmosphere for 2 h and cooled to room temperature under N_2 atmosphere. Finally, this sample was post-annealed at 500 ℃ or 700 ℃ under H_2/Ar atmosphere for another 2 h to obtain structurally disordered Pt_3Fe (denoted as D-Pt_3Fe) and structurally ordered Pt_3Fe (denoted as O-Pt_3Fe), respectively. PtFe and $PtFe_3$ nanoparticles were also prepared using the same procedure.

Physical characterization

The as-prepared nanoparticles were characterized by powder X-ray diffraction (XRD) using an X' Pert PRO diffractometer, and diffraction patterns were collected at a scanning rate of 4 ° min^{-1} and with a step of 0.02 °. The composition of the catalysts was determined by X-ray Fluorescence (XRF) using an EAGLE III spectrometer. Transmission electron microscopy (TEM) was performed using a Tecnai G2 20 operated at 200 kV. The XAFS spectra at Pt L_3-edge (E_0 = 11564 eV) and Fe K-edge (E_0 = 7112 eV) were performed at the beamline 8-ID of the National Synchrotron Light Source II (Brookhaven National Laboratory, NY, USA). The energy of Pt samples and Fe samples was calibrated accordingly to the absorption edge of pure Pt foil and pure Fe foil.

Electrochemical measurement.

All of the electrochemical measurements were performed at room temperature using an Autolab PG302N Potentiostat/Galvanostat and a three-electrode electrochemical cell. The working electrode was used a glassy carbon disk with 5 mm in diameter. 5 mg of samples were dispersed in 1 mL isopropanol/Nafion hybrid solutions via ultrasonic dispersion to form a homogeneous ink. 3 μL of ink was dropped onto the glassy carbon electrode, and dried naturally. The Pt loadings of the catalysts on the electrode were calculated to be 15 μg cm^{-2}. A Pt wire was used as the counter electrode, and a reversible hydrogen electrode (RHE) was used as the reference electrode. The catalysts were first subject to cyclic voltammetry (CV) scans between 0.05 and 1.2 V at 200 mV s^{-1} in N_2-saturated 0.1 M $HClO_4$ until a stable CV was obtained (typically 50 cycles). For the ECSA study, CV was conducted over a potential range from 0.05 and 1.2 V at a scan rate of 50 mV s^{-1} in 0.1 M $HClO_4$. ECSA values were calculated by integrating the area under the curve for the hydrogen adsorption/desorption region between 0.05 and 0.4 V for the reverse sweep in the cyclic voltammetry and using a conversion factor of 210 μC cm^{-2} for the adsorption of a monolayer of hydrogen. ORR polarization curves were recorded by linear-sweep voltammetry (LSV) from 0.2 to 1.05 V at a scan rate of 5 mV s^{-1} in O_2-saturated 0.1 M $HClO_4$ with the GC-RDE rotating at 1600 rpm. Accelerated durability tests (ADT) of the catalysts for ORR were conducted in N_2-saturated or O_2-saturated 0.1 M $HClO_4$ for 10,000 potential cycles between 0.6 and 1.0 V at 0.1 V s^{-1}.

Results and discussion

Density function theory (DFT) calculations were firstly performed to rationalize the specific activity sequence of ordered Pt-Fe model with common crystal face (111)[24-27] towards ORR and shown in **Figure 1a-b**. The Perdew, Burke and Ernzerhof (PBE) function

relaxed lattice constants for *fcc* structured Pt_3Fe and $PtFe_3$ are 3.9335 Å and 3.7269 Å, respectively, in line with that more Fe

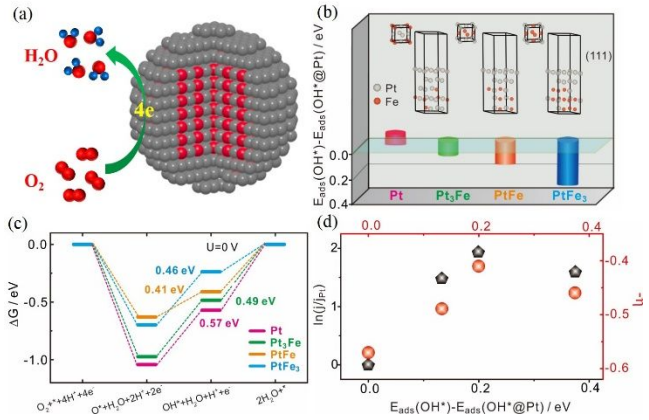

Figure 1. (a) Schematic diagram of ORR on Pt-rich O-PtFe model. (b) Structures of the slab model which were adopted to simulate the ordered Pt-Fe catalysts and the adsorption energy of OH* on the Pt (111) surface. (c) Free energy diagram at zero potential for different intermediate states of ORR for ordered Pt-Fe and pure Pt. (d) The relationship between OH* adsorption strength relative to that of Pt and kinetic current density (black) as well as overpotential (red) of ordered Pt-Fe.

content leads to smaller lattice constant. For the *fct* structured PtFe (O-PtFe), the lattice constants are a = b = 3.9053 Å while c = 3.7057 Å. The adsorption energy of OH* on the (111) surface of O-Pt_3Fe, O-PtFe and O-$PtFe_3$ are calculated with referenced to OH* on Pt (111). It was shown that more Fe content leads to a weaker OH* binding strength. **Figure 1c** is the calculated free energy includes the electronic energy and the zero-point energy from DFT. The solvation correction for OH* is applied according to the reference[28]. The computational hydrogen electrode model was used to calculate the chemical potential of electron and proton, which means $\mu(e^-)+\mu(H^+) = 1/2\ \mu(H_2)$ - eU[29]. It can be seen that the O-PtFe (0.41 eV) and O-$PtFe_3$ (0.46 eV) present obviously lower energy barrier than order O-Pt_3Fe (0.49 eV) and pure Pt (0.57 eV) of their own rate-limiting step. **Figure 1d** plots the relationship between kinetic current density (over potential) and OH* adsorption strength calculated by DFT, it shows volcano curves and the top of the volcano curve corresponds to the optimal adsorption strength of O-PtFe with 2-3 atomic layers of Pt. All the DFT calculations indicate collectively that PtFe nanoparticles with ordered core and Pt skin are beneficial to catalyze the ORR.

For the preparation of the desired O-PtFe with 2-3 atomic layers of Pt, carbon supported PtFe nanoparticles were prepared by an impregnation-reduction method and followed by a post-annealing process in H_2/Ar (7% H_2, volume ratio) atmosphere[30, 31]. The XRD patterns display in **Figure 2a** show that the PtFe annealed at 500 °C exhibits a typical disordered *fcc* alloy feature (D-PtFe), four diffraction peaks (111), (200), (220), and (311) are agree with those of the Pt with peaks shifting to higher angles. After heat-treatment at 700 °C for 2 h, additional (001), (110), (002), (201), (112), (202), (221) and (310) peaks, which are characteristics of an ordered intermetallic PtFe phase (PDF card # 03-065-1051) with *fct* structure were appeared, indicate the formation of O-PtFe. The typical TEM image of the carbon supported O-PtFe as shown in **Figure 2b**, from which we can see that all the nanoparticles are uniformly dispersed on carbon support with the average size of 6 nm based on the statistic of more than 200 particles. An individual O-PtFe nanoparticles with the interplanar spacing (0.3718 nm) in line with (001) plane of Pt was viewed along the [010] zone axis as shown in **Figure 2c** and the inset shows the diffractogram of the nanoparticle projected along the [110] axis, confirming the ordered intermetallic core and the ultrathin Pt shell. Line scanning (**Figure 2d)** which crossing a nanoparticle and elemental mapping (**Figures e-f)** prove that Pt (red) versus Fe (green) are uniformly distributed and a core-shell structure with ultrathin Pt shell (ca. 0.4 nm, 2-3 atomic layers) was formed. Meanwhile, carbon supported O-Pt_3Fe and O-$PtFe_3$ were also prepared via the same method except the Pt to Fe ratio in the precursor. The structural and morphological characterizations of them are shown in **Figures S1-3** and **Table S1**. All of the results prove that the desired O-PtFe with ultrathin Pt shell were successfully obtained by our synthetic method. Generally, such ordered intermetallic core with contracted Pt shell will lead to a weaker OH* binding strength, which would be favorable to ORR[13].

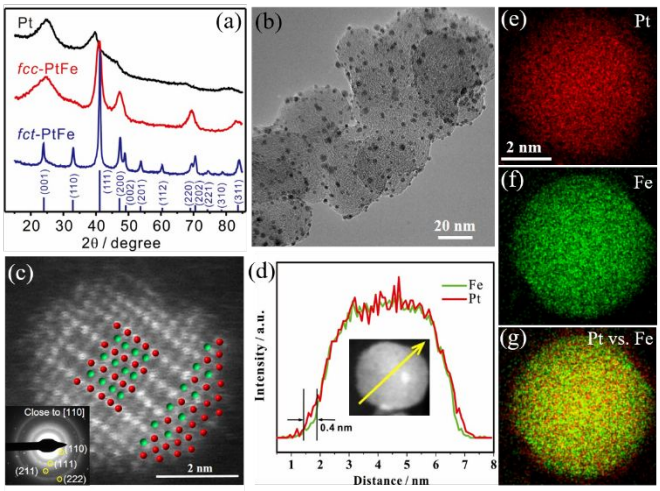

Figure 2. (a) XRD patterns of carbon supported Pt, D-PtFe and O-PtFe. (b) TEM image of O-PtFe. (c) The atomic-resolution HAADF-STEM image of O-PtFe with 2-3 atomic layers of Pt (red), the inset shows the diffractogram of a nanoparticle projected along the [110] axis. STEM-EELS line-scanning (d) and elemental mapping (e-g) images of O-PtFe nanoparticle.

Electrochemical measurements were conducted to determine the electrochemically active surface areas (ECSA) and ORR activities of these catalysts. **Figure 3a** compares cyclic voltammograms (CVs) and the linear sweep voltammetry (LSV) of Pt, D-PtFe and O-PtFe. The activity, which measured by half wave potentials ($E_{1/2}$) of LSV, increases in the following order of Pt (0.862 V) < D-PtFe (0.909 V) < O-PtFe (0.921 V). While the ECSA increases in the inverse order of O-PtFe (29.7 m^2/g_{Pt}) < D-PtFe (46.1 m^2/g_{Pt}) < Pt (60.3 m^2/g_{Pt}). The smaller ECSA of D-PtFe and O-PtFe mainly because of their larger size compared with Pt (ca. 2 nm) (**Figures S4-5**). Taking into account the lowest ECSA of O-PtFe and the highest activity it delivered, it

could be confirmed that the dramatic catalytic enhancement effect of the ordered core and Pt shell on ORR[32]. Tafel plots of these

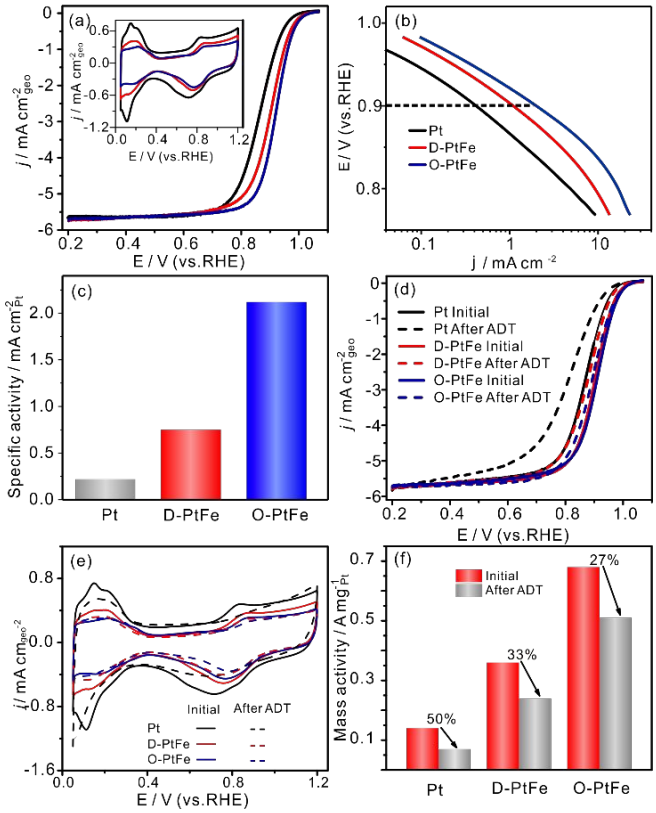

Figure 3. (a) LSV curves of carbon supported O-PtFe, D-PtFe and Pt, inset are the corresponding CVs. Tafel plots (b) and SA at 0.9 V (c) for ORR on O-PtFe, D-PtFe and Pt. The LSV curves (d), CVs (e) and mass activity (f) of Pt, D-PtFe, O-PtFe before and after ADT.

catalysts are depicted in **Figure 3b**, all of them display slopes of ca. -58 mV/dec at low overpotential region and ca. -108 mV/dec at high overpotential region, indicating that the rate-determining step of ORR involved charge transfer and migration of reaction intermediates[33], respectively. Their kinetic current density (j_k) were obtained from the LSV according to Koutecky-Levich equation and used to obtain specific activity (SA, normalized to ECSA of Pt) and mass activity (MA, normalized to Pt loading), as shown in **Figure 3c** and **3f**, respectively. At +0.9 V, the O-PtFe (2.23 mA cm^{-2}_{Pt}) presents enhanced SA than that on D-PtFe (0.79 mA cm^{-2}_{Pt}) and Pt (0.23 mA cm^{-2}_{Pt}) and the specific activity delivered by O-PtFe in this work was also competitive in comparision with other Pt-based intermetallic ORR catalysts reported previously (**Table S2**). Additionally, the eletrocatalytic activity of the other Pt-Fe series catalysts were also evaluated and summarized in **Figures S6-9**. All of Pt-Fe catalysts exhibited lower ORR over-potential and higher half wave potentials than Pt, suggesting that the alloying Pt with Fe leads to an increased activity. Moreover, the ordered intermetallics displayed better performance than their disordered counterparts, further confirmed that the ordered structure have optimized adsorptions of oxygen species like O*, OH* and etc. on the active surface, resulting in further enhanced activity towards ORR.

Since long-term durability of catalyst is another critical parameter for PEMFCs application, ADT was conducted to evaluate the durability of these catalysts in O_2-saturated 0.1 M $HClO_4$ and potential cycling between 0.6 and 1.0 V, which is close to the practical potential range at FCs cathode. The LSVs and CVs of these catalysts before and after 10000 potential cycles are summarized in **Figure 3d-e**. For O-FePt, the LSV exhibits negligible negative shift of its $E_{1/2}$ after ADT, as contrast, D-FePt and Pt show 22 and 35 mV negative shift, respectively. The ECSA of O-FePt, D-FePt and Pt after ADT are calculated to be 40.7, 39.5 and 28.9 m^2 g_{Pt}^{-1}, respectively. We can see that there is a ECSA increase for O-PtFe due to the slight Fe dissolution on the surface and more Pt active sites are exposed, while the ECSA of D-PtFe and Pt decrease more after ADT. because of the drastic Fe dissolution and/or Ostwald growth (**Figures S10-11**), further confirming the enhanced Fe anti-leaching ability of the *fct* intermetallics[34, 35]. Moreover, after 10000 potential cycles, the mass activities of the O-PtFe (0.50 A/mg_{Pt}), D-PtFe (0.24 A/mg_{Pt}) and Pt (0.07 A/mg_{Pt}) decayed 27%, 33% and 50% of their initial value, respectively. All of the results indicate that the remarkable durability of O-PtFe in the ORR test condition (**Figures S12-14**). To evidence the remarkable stability of O-PtFe, the catalysts, which loaded on carbon paper and cycled between 0.6-1.0 V for ADT were investigated by XRF and XRD. It can be seen that O-PtFe showed smaller Fe leaching than D-PtFe (**Figure S15**). As predicated, the bulk structure of D-PtFe was changed severely due to the dissolution of Fe while O-PtFe had a good retention of its initial fct structure (**Figure S16**).

Apart from the ex-situ characterization, we further carried out in-situ X-ray absorption fine structure spectroscopy (in-situ XAFS) at Pt L_3-edge to probe the local and electronic structures change of the O-PtFe during 10k ADT cycles (**Figure 4a**). We can see that the initial normalized Pt L_3-edge X-ray absorption near edge structure (XANES) spectra (**Figure 4b**) in both O-PtFe and D-PtFe are mainly in metallic state (Pt^0) and the slightly negative shift demonstrating that the d-electron density of Pt is reduced due to the alloy with the metallic Fe, in agreement with the results reported previously[23, 36]. The Pt-Pt coordination number (CN) is 7.0 while the Fe-Fe CN is just about 2.5 (**Figure 4c** and **Table S3**) suggesting that the Fe-Fe bonding is localized in 2D while the Pt-Fe bonding is in 3D. Furthermore, the bond length of Pt-Pt (2.708 Å) is shorter than bulk Pt-Pt (2.775 Å) mainly due to the incorporation of Fe atoms with Pt. The total Fe CN (ca. 2.6), which is smaller than the total Pt CN (ca. 7) also providing evidence that Pt-rich on the surface of the O-PtFe[37]. The Pt L_3-edge EXAFS spectra and XANES spectra during ADT were recorded and plotted in **Figure 4d-e** indicates the ordered structure is maintained to a great extent[23], in both intensity and peak position. Whlie the Fe K-edge XANES spectra witnessed slightly decrease (**Figure S17**) due to the surface Fe leaching meanwhile Pt skin was formed gradually. The CN and bond length in O-PtFe during 10000 cycles (**Figure S18**) were also fitted and listed in **Table S4**, no significant changes further proving the excellent durability of O-PtFe under typical potential range at FCs cathode, in consistent with the ex-situ XRF and XRD results aforementioned.

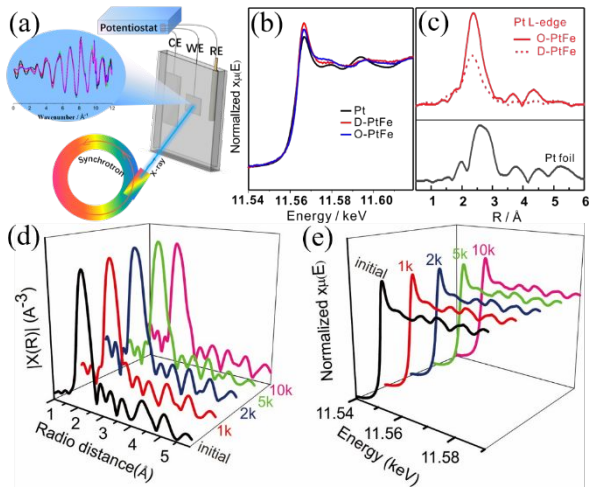

Figure 4. (a) Schematic diagram of in-situ XAFS experiment during ADT. Pt L_3-edge XANES (b) and EXAFS (c) profiles of Pt, D-PtFe, O-PtFe. Pt L_3-edge EXAFS (d) and XANES (e) spectra of O-PtFe under ADT cycles.

Conclusions

In conclusion, an ordered intermetallic structure *fct*-PtFe nanoparticle with ultrathin Pt shell has been successfully synthesized. Concrete evidence indicate that the ordered *fct*-PtFe core with 2-3 atomic layer compressed Pt shell is more active and stable towards ORR than the corresponding D-PtFe and Pt. In-situ XAFS experiment shows that the unique structure of O-PtFe not only lead to a weaker OH* binding strength (beneficial to activity), but also chemically stable against Fe leaching (beneficial to durability). We hope the facile, scalable synthesis method and in-situ XAFS experiment could be readily adapted to other catalyst system, facilitating the screening of highly efficient ORR catalysts for fuel cells.

Acknowledgements

This work was supported by National Natural Science Foundation (21573083), 1000 Young Talent (to Deli Wang) and the Innovation Research Funds of Huazhong University of Science and Technology (2017KFYXJJ164). We thank the Analytical and Testing Center of Huazhong University of Science and Technology for its facilities and help. The S/TEM and computational work was carried out at the Center for Functional Nanomaterials, Brookhaven National Laboratory, which supported by the U.S. Department of Energy, Office of Basic Energy Sciences, under Contract No. DE-SC0012704. The XAFS research used beamline 8-ID of the National Synchrotron Light Source II, a U.S. Department of Energy (DOE) Office of Science User Facility operated for the DOE Office of Science by Brookhaven National Laboratory under Contract No. DE-SC0012704. M. X. Gong thanks the scholarship supported by the China Scholarship Council (CSC) (201706160151).

Notes and references

1. M. Shao, Q. Chang, J. P. Dodelet and R. Chenitz, *Chem. Rev.*, 2016, **116**, 3594-3657.
2. C. Koenigsmann, A. C. Santulli, K. Gong, M. B. Vukmirovic, W. P. Zhou, E. Sutter, S. S. Wong and R. R. Adzic, *J. Am. Chem. Soc.*, 2011, **133**, 9783-9795.
3. Y. Nie, L. Li and Z. Wei, *Chem. Soc. Rev.*, 2015, **44**, 2168-2201.
4. K. Sasaki, H. Naohara, Y. Choi, Y. Cai, W.-F. Chen, P. Liu and R. R. Adzic, *Nat. Commun.*, 2012, **3**, 1115.
5. S. Guo, S. Zhang and S. Sun, *Angew. Chem. Int. Ed.*, 2013, **52**, 8526-8544.
6. J. Wu and H. Yang, *Acc. Chem. Res.*, 2013, **46**, 1848-1857.
7. B. Lim, M. Jiang, P. H. Camargo, E. C. Cho, J. Tao, X. Lu, Y. Zhu and Y. Xia, *Science*, 2009, **324**, 1302-1305.
8. C. Chen, Y. Kang, Z. Huo, Z. Zhu, W. Huang, H. L. Xin, J. D. Snyder, D. Li, J. A. Herron and M. Mavrikakis, *Science*, 2014, **343**, 1339-1343.
9. X. Huang, Z. Zhao, L. Cao, Y. Chen, E. Zhu, Z. Lin, M. Li, A. Yan, A. Zettl and Y. M. Wang, *Science*, 2015, **348**, 1230-1234.
10. L. Tang, B. Han, K. Persson, C. Friesen, T. He, K. Sieradzki and G. Ceder, *J. Am. Chem. Soc.*, 2009, **132**, 596-600.
11. J. Kim, Y. Lee and S. Sun, *J. Am. Chem. Soc.*, 2010, **132**, 4996-4997.
12. D. Y. Chung, S. W. Jun, G. Yoon, S. G. Kwon, D. Y. Shin, P. Seo, J. M. Yoo, H. Shin, Y. H. Chung, H. Kim, B. S. Mun, K. S. Lee, N. S. Lee, S. J. Yoo, D. H. Lim, K. Kang, Y. E. Sung and T. Hyeon, *J. Am. Chem. Soc.*, 2015, **137**, 15478-15485.
13. T. Ghosh, M. B. Vukmirovic, F. J. DiSalvo and R. R. Adzic, *J. Am. Chem. Soc.*, 2009, **132**, 906-907.
14. M. Luo, Y. Sun, L. Wang and S. Guo, *Adv. Energy Mater.*, 2017, **7**, 1602073.
15. M. Luo and S. Guo, *Nat. Rev. Mater*, 2017, **2**, 17059.
16. G. Wang, B. Huang, L. Xiao, Z. Ren, H. Chen, D. Wang, H. D. Abruña, J. Lu and L. Zhuang, *J. Am. Chem. Soc.*, 2014, **136**, 9643-9649.
17. Y. Yan, J. S. Du, K. D. Gilroy, D. Yang, Y. Xia and H. Zhang, *Adv. Mater.*, 2017, **29**.
18. W. Xiao, W. Lei, M. Gong, H. L. Xin and D. Wang, *ACS Catal.*, 2018, **8**, 3237-3256.
19. D. Wang, H. L. Xin, R. Hovden, H. Wang, Y. Yu, D. A. Muller, F. J. DiSalvo and H. D. Abruna, *Nat. Mater.*, 2013, **12**, 81-87.
20. Z. Cui, H. Chen, M. Zhao, D. Marshall, Y. Yu, H. Abruna and F. J. DiSalvo, *J. Am. Chem. Soc.*, 2014, **136**, 10206-10209.
21. G. Jiang, H. Zhu, X. Zhang, B. Shen, L. Wu, S. Zhang, G. Lu, Z. Wu and S. Sun, *ACS nano*, 2015, **9**, 11014-11022.
22. Q. Li, L. Wu, G. Wu, D. Su, H. Lv, S. Zhang, W. Zhu, A. Casimir, H. Zhu, A. Mendoza-Garcia and S. Sun, *Nano Lett.*, 2015, **15**, 2468-2473.
23. J. Li, Z. Xi, Y. T. Pan, J. S. Spendelow, P. N. Duchesne, D. Su, Q. Li, C. Yu, Z. Yin, B. Shen, Y. S. Kim, P. Zhang and S. Sun, *J. Am. Chem. Soc.*, 2018, **140**, 2926-2932.
24. G. Kresse and J. Furthmüller, *Phys. Rev. B*, 1996, **54**, 11169.
25. P. E. Blöchl, *Phys. Rev. B*, 1994, **50**, 17953.
26. G. Kresse and D. Joubert, *Phys. Rev. B*, 1999, **59**, 1758.
27. K. Burke, M. Ernzerhof and J. P. Perdew, *Chem. Phys. Lett.*, 1997, **265**, 115-120.
28. G. Karlberg, J. Rossmeisl and J. K. Nørskov, *Phys. Chem. Chem. Phys.*, 2007, **9**, 5158-5161.
29. J. K. Nørskov, J. Rossmeisl, A. Logadottir, L. Lindqvist, J. R. Kitchin, T. Bligaard and H. Jonsson, *J. Phys. Chem. B*, 2004, **108**, 17886-17892.
30. D. Wang, Y. Yu, J. Zhu, S. Liu, D. A. Muller and H. D. Abruna, *Nano Lett.*, 2015, **15**, 1343-1348.

31. J. Zhu, X. Zheng, J. Wang, Z. Wu, L. Han, R. Lin, H. L. Xin and D. Wang, *J. Mater. Chem A*, 2015, **3**, 22129-22135.
32. J. Li, S. Sharma, X. Liu, Y.-T. Pan, J. S. Spendelow, M. Chi, Y. Jia, P. Zhang, D. A. Cullen and Z. Xi, *Joule*, 2018.
33. C. Coutanceau, M. Croissant, T. Napporn and C. Lamy, *Electro. Acta*, 2000, **46**, 579-588.
34. G.-F. Wei and Z.-P. Liu, *Energy Environ. Sci*, 2011, **4**, 1268-1272.
35. D. Li, C. Wang, D. Tripkovic, S. Sun, N. M. Markovic and V. R. Stamenkovic, *ACS Catal.*, 2012, **2**, 1358-1362.
36. P. N. Duchesne, G. Chen, N. Zheng and P. Zhang, *J. Phys. Chem. C*, 2013, **117**, 26324-26333.
37. J. Durst, M. Lopez-Haro, L. Dubau, M. Chatenet, Y. Soldo-Olivier, L. Guétaz, P. Bayle-Guillemaud and F. d. r. Maillard, *J. Phys. Chem. Lett.*, 2014, **5**, 434-439.

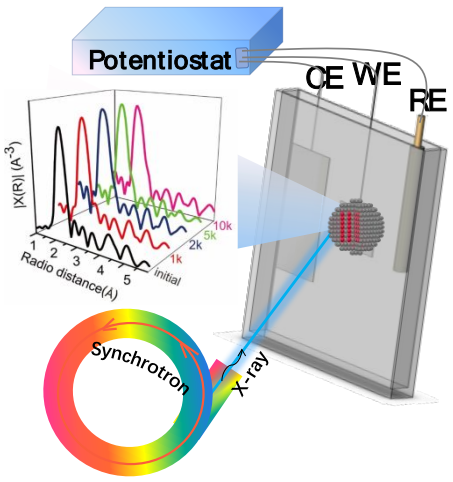

The ordered PtFe with atomic Pt shell has been successfully synthesized and deliver enhance performance towards ORR.